A Joint Experimental and Theoretical Study on the Mechanisms of Methyl 2-Hydroxypropionate and Methyl 2-Hydroxyisobutyrate Decomposition in the Gas Phase

Vicent S. Safont,* Juan Andrés, and Raquel Castillo

Departament de Ciències Experimentals, Universitat Jaume I, Box 224, 12080 Castelló, Spain

Gabriel Chuchani, Alexandra Rotinov, Rosa M. Domínguez, and Armando Herize

Centro de Química, Instituto Venezolano de Investigaciones Científicas, Apartado 21827, Caracas 1020-A, Venezuela

Received: August 19, 2003; In Final Form: October 27, 2003

The gas-phase decomposition kinetics of the title compounds have been examined over the temperature range of 369.9−439.4 °C and pressure range of 67.5−209.0 Torr. The reactions were found to be homogeneous and unimolecular and to follow a first-order rate law. The rate coefficients are expressed by the following Arrhenius equations: for methyl 2-hydroxypropionate (**I**), $\log k_1\ (s^{-1}) = (13.73 \pm 0.19) - (219.8 \pm 2.5)$ kJ·mol^{-1} $(2.303RT)^{-1}$, and for methyl 2-hydroxyisobutyrate (**II**), $\log k_1\ (s^{-1}) = (13.37 \pm 0.39) - (217.1 \pm 5.1)$ kJ·mol^{-1} $(2.303RT)^{-1}$. The decomposition products of **I** are acetaldehyde, methanol, and carbon monoxide, while **II** yields mainly acetone, methanol, and carbon monoxide and very small amounts of methyl formate and methyl methacrylate. The reaction mechanisms have been theoretically characterized at B3LYP/6-31+G**, MP2/6-31G**, and MP2/6-31++G** computing levels by characterizing the stationary points (reactants, products, intermediates, and transition structures) on the potential energy surface. The transition-state theory has been used to obtain the rate coefficients, and a good agreement is found between theoretical and experimental results.

1. Introduction

Gas-phase experiments provide the opportunity to obtain valuable information on elementary reactions and mechanisms in a controlled environment without disturbing factors such as the presence of solvent molecules. In this context, the gas-phase thermal decomposition of several carboxylic acids derivatives was studied by some of us.[1−8] From an experimental point of view, explicit information on the elementary steps involved along the whole reaction path is often difficult to obtain, and a closer interaction between theory and experiment has turned out to be very fruitful in this area of chemistry. The availability of experimental data concerning the activation parameters, in particular, rate coefficients and activation energies, made it possible to check the reliability of quantum chemical tools in the description of these processes. Therefore, the kinetics of the gas-phase thermal decompositions of 2-chloropropionic,[9] glycolic, lactic, 2-hydroxyisobutyric,[10] mandelic,[11] and methoxyacetic, ethoxyacetic, and isopropoxyacetic[12] acids was theoretically studied. In addition, the gas-phase decompositions of 2-methoxypropionic, 2-ethoxypropionic, 2-isopropoxypropionic,[13] and 3-chloropivalic[14] acids were studied by means of combined experimental and theoretical approaches.

The 2-chloropropionic acid decomposition[1,9] takes place along a two-step mechanism; in the first and rate-limiting step, the hydrogen chloride is formed via a (3.1.0) bicyclic transition structure (TS) with participation of the carbonylic oxygen of the carboxyl group and the assitance of the acidic hydrogen, thus yielding an α-propiolactone intermediate. This, in turn, decomposes to carbon monoxide and acetaldehyde (Scheme 1). The same mechanism has been found to preferentially take place if the 2-substituent is a hydroxyl group[3,7,10,11] or an alkoxy group[6,12,13] and has been proposed as the preferred mechanism for other 2-chloroacids,[4,15] 2-bromoacids,[2,5] and 2-phenoxyacids.[8]

SCHEME 1: Schematic Description of the Two-Step Mechanism for the Decomposition of 2-Substituted Carboxylic Acids

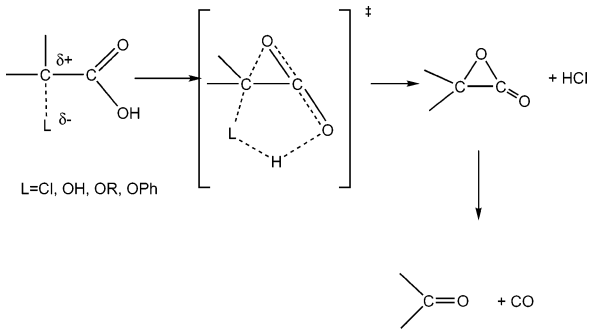

The assistance of the H of the COOH to the leaving L group and the nucleophilic participation of the oxygen carbonyl for the lactone formation may be derived from the results in the pyrolyses of 2-chloro- and 2-bromopropionic acids as compared with the results of the decomposition of their methyl esters.[1,2] Since neighbor group participation in liquid media and in the gas phase has been reported,[16,17] it was thought that with replacement of the H of the COOH by the methyl group in the haloacids, the carbon−halogen bond polarization, in the sense $C^{\delta+}\cdots X^{\delta-}$, may first be assisted anchimerically by the carbo-

* To whom correspondence should be addressed. E-mail: safont@exp.uji.es. Telephone: 34 964728085. Fax: 34 964728066.

10.1021/jp030985h CCC: $27.50
Published on Web 01/14/2004

SCHEME 2: Schematic Description of the Expected Two-Step Mechanism for the Decomposition of 2-Substituted Methyl Esters

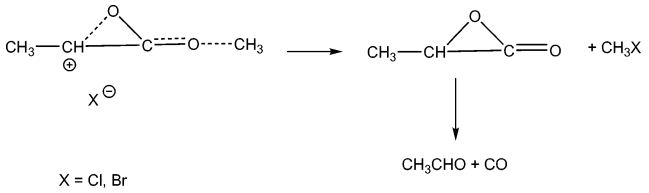

nylic oxygen. Therefore, the leaving X group, through an intramolecular solvation or autosolvation, may uptake the methyl group of the ester to give CH_3X as described in Scheme 2. However, the products of direct elimination, that is, the corresponding alkene and HX, are obtained.[2,18] This fact suggests that the assistance of the H of the COOH to the leaving group is necessary in the process of elimination to yield the lactone intermediate.

The OH group of aliphatic alcohols is known to be a very poor leaving group, especially in dehydration processes; therefore, it is interesting to determine the gas-phase elimination kinetics of 2-hydroxycarboxylic acids with the H of the COOH replaced by the methyl group, that is, primary, secondary, and tertiary methyl esters of 2-hydroxycarboxylic acids. This type of compound may provide information as to whether the oxygen carbonyl provides anchimeric assistance or some other type of mechanism may occur during the pyrolytic decomposition. In addition to the experiments, theoretical calculations have been done to obtain a more adequate interpretation about the mechanistic pathways of these reactions.

The aim of the present study is to extend our work on this type of compound, and here we report the experimental kinetics of the decomposition processes of methyl hydroxyacetate, methyl 2-hydroxypopionate (**I**), and methyl 2-hydroxyisobutyrate (**II**). We also report a detailed theoretical study of the corresponding reaction pathways for the decomposition of **I** and **II**. A comparison between experimental and theoretical values of activation parameters has been carried out.

2. Experimental Section

Methyl 2-Hydroxyacetate (Methyl Glycolate). This compound was bought from Aldrich of 98% purity (GLC, FFAP-7% Chromosorb AW DMCS 80−100 mesh). The decomposition products are acetaldehyde (Aldrich), methanol (Aldrich), CO_2, and CO. The analyses were irreproducible and could not be estimated quantitatively in the same FFAP or any other column.

Methyl 2-Hydroxypropionate (Methyl Lactate). This substrate (Aldrich) of 99.9% purity determined by GLC (FFAP-7% Chromosorb AW DMCS 80−100 mesh) was used. The products acetaldehyde (Aldrich) and methanol (Aldrich) were quantitatively analyzed in the same FFAP column.

Methyl 2-Hydroxyisobutyrate. Methyl 2-hydroxyisobutyrate was found to be of 98.7% purity (GLC, Porapak R 80−100 mesh). The pyrolysis product acetone (Merck) was quantitatively analyzed in the Porapak R column. The identities of the substrates and products were additionally verified by mass spectrometry and nuclear magnetic resonance spectroscopy.

Kinetics. The kinetic experiments were carried out in a static reaction apparatus as described before[19,20] but with some modifications and additions of modern electronic and electrical devices. The reaction vessel was seasoned with allyl bromide, and the pyrolysis was performed in the presence of cyclohexene or toluene as a free radical chain inhibitor. The temperature was controlled by a resistance thermometer controller type SHINKO DC-PS 25RT and an OMEGA solid-state relay, model SSR240 AC45, maintained within ±0.20 °C and measured with a calibrated platinum−platinum−13% rhodium thermocouple. No temperature gradient was found along the reaction vessel. The rate coefficients of methyl 2-hydroxypropionate were determined by the unreacted amount of the substrate through chromatographic analyses (OV 101−10% Gas Chrom. QI 80−100 mesh). In the case of methyl 2-hydroxyisobutyrate, the kinetics was followed by quantitative analyses of acetone formation in the column of Porapak R 80−100 mesh. The substrates were injected with a syringe through a silicone rubber septum directly into the reaction vessel.

3. Computing Methods

The transition state theory (TST)[21,22] was devised to facilitate the interpretation of rate coefficients and is used almost universally by chemists interested in reaction mechanisms. Other theories have been developed to calculate the rate coefficients for chemical processes,[23] such as the Rice-Ramsperger-Kassel-Marcus (RRKM)[24,25] or the variational transition-state theory (VTST);[26,27] however the mechanism of a given chemical reaction can be described by the transition structure associated with the chemical interconversion step in the sense proposed by Tapia and Andrés.[28,29] We have selected this method to calculate the kinetic parameters in the present study.

Calculations at the MP2 level of theory with the 6-31G** and 6-31++G** basis sets have been performed with the Gaussian 98[30] program. In addition, the B3LYP/6-31+G** level has also been used. The Berny analytical gradient optimization routines[31,32] were used for optimization. The requested convergence on the density matrix was 10^{-9} atomic units; the threshold value of maximum displacement was 0.0018 Å, and that of maximum force was 0.000 45 hartree/bohr. The nature of each stationary point was established by calculating and diagonalizing the Hessian matrix (force constant matrix). The TSs were characterized by means of a normal-mode analysis. The unique imaginary frequency associated with the transition vector (TV),[33] that is, the eigenvector associated with the unique negative eigenvalue of the force constant matrix, has been characterized. The intrinsic reaction coordinate (IRC)[34] path was traced to check and obtain the energy profiles connecting each transition structure to the two associated minima of the proposed mechanism by using the second-order González−Schlegel integration method.[35,36]

Each stationary point in the potential energy surface (PES) is characterized by an index that is equal to the number of negative eigenvalues of the Hessian matrix (0 for a minimum, 1 for a saddle point). This index is also the number of imaginary wavenumbers obtained in a normal-mode analysis of the corresponding molecular structure. This analysis also provides thermodynamic quantities such as zero-point vibrational energy (ZPVE), temperature corrections ($E(T)$), and the absolute entropy ($S(T)$),[37] and consequently, the rate coefficient can be estimated. Temperature corrections and absolute entropies were obtained assuming ideal gas behavior from the harmonic frequencies and moments of inertia by standard methods.[38] A temperature of 673.15 K (400 °C), inside the experimental range, was taken in the calculations.

The first-order rate coefficient ($k(T)$) was computed using the TST[21,39] and assuming that the transmission coefficient is equal to 1, as expressed by the following relation:

$$k(T) = (kT/h)\exp(-\Delta G^{\ddagger}/(RT)) \qquad (1)$$

TABLE 1: Stoichiometry of the Decomposition Reaction[a]

substrate	T (°C)	params	value				
methyl 2-hydroxy-propionate[b]	399.4	time (min)	5	10	15	20	25
		reaction (%) (pressure)	11.9	21.7	30.3	39.2	56.4
		substrate (%) (GLC)[d]	12.0	22.2	32.4	39.7	57.3
methyl 2-hydroxy-isobutyrate[c]	419.7	time (min)	4	5	6.5	8	10
		reaction (%) (pressure)	26.0	24.2	33.4	38.0	43.5
		substrate (%) (GLC)	26.2	29.1	33.5	37.3	42.7

[a] Vessel seasoned with allyl bromide. [b] In the presence of toluene inhibitor. [c] In the presence of cyclohexene inhibitor. [d] GLC = gas−liquid chromatography.

in which $\Delta G^{\ddagger}$ is the Gibbs free energy change between the reactant and its corresponding transition structure and k and h are the Boltzmann and Planck constants, respectively. $\Delta G^{\ddagger}$ was calculated as usually:

$$\Delta G^{\ddagger} = \Delta H^{\ddagger} - T\Delta S^{\ddagger} \quad (2)$$

and

$$\Delta H^{\ddagger} = \mathrm{PEB} + \Delta\mathrm{ZPVE} + \Delta E(T) \quad (3)$$

where $\Delta H^{\ddagger}$ is the activation enthalpy, PEB is the potential energy barrier, and ΔZPVE and $\Delta E(T)$ are the differences of ZPVE and temperature corrections between the TS and the corresponding reactant, respectively. $\Delta S^{\ddagger}$ is obtained directly as the entropy (taken from the normal mode Gaussian 98 outputs) difference between the TS and its corresponding reactant.

4. Results and Discussion

4.1. Experimental Results. The gas-phase elimination of methyl 2-hydroxyacetate (methyl glycolate) in a vessel seasoned with allyl bromide and in the presence of the free radical inhibitor toluene was found to be difficult for complete kinetic mesurements. At two different temperatures, it was possible to determine approximately the overall rate coefficients: $k = 0.68 \times 10^{-4}$ s^{-1} (420.0 °C) and $k = 2.16 \times 10^{-4}$ s^{-1} (439.7 °C). Moreover, yields of products CH_3OH, CH_2O, CO, CO_2, and CH_4 were erratic and irreproducible. This elimination process showed to be rather complex with concurrent molecular and radical reactions.

The pyrolysis products of **I** in a vessel seasoned with allyl bromide and in the presence of the inhibitor toluene were acetaldehyde, methanol, and carbon monoxide:

$$CH_3CH(OH)COOCH_3 \rightarrow CH_3CHO + CH_3OH + CO \quad (4)$$

The stoichiometry of reaction 4 was made by comparing, up to 60% decomposition, the percentage decomposition of the substrate from pressure measurements with those obtained from the quantitative chromatographic analyses of the reacted amount of the ester (Table 1).

The homogeneity of the reaction was examined by using a vessel with a surface-to-volume ratio of 6.0 times greater than that of the unpacked vessel (Table 2). The rates were found to be unaffected by the packed and unpacked seasoned vessels, while a significant heterogeneous effect was obtained in the packed and unpacked clean Pyrex vessels. The effect of the free radical inhibitor cyclohexene is shown in Table 3. The kinetic runs had to be carried out with at least an equal amount of cyclohexene to suppress any possible free radical process of the starting material or product or both. No induction period was observed: when the substrate was introduced into the reaction vessel, the process of elimination immediately took place. Moreover, drawing the graph of total pressure (mmHg) versus time (min), we obtained a curve characteristic of a unimolecular reaction. Also, the presence of different proportions of free radical inhibitors (Table 3) did not affect the rate coefficient. The k-values are reproducible with a standard deviation not greater than 5% at a given temperature.

TABLE 2: Homogeneity of the Reaction

substrate	T (°C)	S/V (cm^{-1})[a]	$10^4 k_1$ (s^{-1})[b]	$10^4 k_1$ (s^{-1})[c]
methyl 2-hydroxy-propionate	399.4	1	8.18[d]	4.45 ± 0.15
		6	12.84[d]	4.26 ± 0.12
methyl 2-hydroxy-isobutyrate	409.9	1	7.51 ± 0.19	6.01 ± 0.11
		6	8.67 ± 0.32	6.19 ± 0.15

[a] S = surface area (cm^2); V = volume (cm^3). [b] Clean Pyrex vessel. [c] Vessel seasoned with allyl bromide. [d] Average k-values.

TABLE 3: Effect of the Free Radical Inhibitor on Rates[a]

substrate	T (°C)	P_s (Torr)	P_i (Torr)	P_i/P_s	$10^4 k_1$ (s^{-1})
I[b]	399.4	130			4.06 ± 0.16
		91	157.5	0.6	4.20 ± 0.10
		126.5	208	1.6	4.50 ± 0.19
		135	355	2.5	4.45 ± 0.15
		82	267.5	3.2	4.81 ± 0.21
II[c]	409.9	105.5			6.66 ± 0.31
		114.0	83.5	0.7	6.41 ± 0.22
		144	174	1.2	6.70 ± 0.28
		104	150	1.4	6.82 ± 0.25
		78	140	3.0	6.49 ± 0.27

[a] P_s = pressure of the substrate; P_i = pressure of the inhibitor. Vessel seasoned with allyl bromide. [b] Inhibitor toluene. [c] Inhibitor cyclohexene.

The experimental stoichiometry for the pyrolytic elimination of **II** in the gas phase (eq 5) was made by comparing, up to 50% reaction, the percentage decomposition of the substrate from pressure measurements with that obtained from the quantitative chromatographic analyses of the unreacted starting material (Table 1).

$$(CH_3)_2C(OH)COOCH_3 \rightarrow CH_3COCH_3 + CH_3OH + CO \quad (5)$$

$$CH_3COCH_3 + HCOOCH_3\ (2\%)^{40}$$

$$CH_2{=}C(CH_3)COOCH_3 + H_2O\ (1\%)$$

The homogeneity of this reaction was established by carrying out several runs in a vessel with a surface-to-volume ratio of 6.0 relative to that of the normal vessel, which is equal to 1.0 (Table 2). The packed and unpacked vessels seasoned with allyl bromide had no effects on rates. However, the packed and unpacked clean Pyrex vessel gave a significant heterogeneous effect in the rate coefficients. The free radical inhibitor toluene had no effect on the rates of elimination (Table 3). No induction period was observed. The rate coeffcients were reproducible with a relative standard deviation of 5% at a given temperature.

The first-order rate coefficients for the pyrolytic elimination of these 2-hydroxyesters, calculated from $k_1 = (2.303/t)\log[P_0/(2P_0 - P_t)]$, were invariant of their initial pressure (Table 4). Plotting $\log[P_0/(2P_0 - P_t)]$ vs time t gave a good straight line up to 60% decomposition for **I** and up to 50% for **II**. The temperature dependence of the rate coefficients and their

TABLE 4: Independence of the Rate Coefficients with Initial Pressure

substrate	T (°C)	params	value				
I	399.9	P_0 (Torr)	67.5	82.5	126.5	157.5	209
		10^4k_1 (s^{-1})	4.24 ± 0.14	4.81 ± 0.21	4.50 ± 0.19	4.20 ± 0.10	4.34 ± 0.13
II	409.9	P_0 (Torr)	76	104	114	149	
		10^4k_1 (s^{-1})	6.49 ± 0.17	6.82 ± 0.25	6.41 ± 0.22	6.10 ± 0.14	

TABLE 5: Variation of Rate Coefficients with Temperature[a]

substrate	parameters	value						
I	T (°C)	369.9	380.0	390.2	399.4	410.0	419.3	429.9
	10^4k_1 (s^{-1})	0.76 ± 0.03	1.41 ± 0.04	2.55 ± 0.09	4.45 ± 0.12	8.31 ± 0.31	14.13 ± 0.51	25.12 ± 0.65
	rate equation $\log k_1$ (s^{-1}) = (13.73 ± 0.19) − (219.8 ± 2.5) kJ·mol^{-1} $(2.303RT)^{-1}$; r = 0.999 92							
II	T (°C)	380.4	390.7	399.8	409.9	419.7	430.2	439.4
	10^4k_1 (s^{-1})	1.09 ± 0.03	1.85 ± 0.06	3.39 ± 0.14	6.01 ± 0.21	10.19 ± 0.30	17.32 ± 0.62	29.46 ± 0.77
	rate equation $\log k_1$ (s^{-1}) = (13.37 ± 0.39) − (217.1 ± 5.1) kJ·mol^{-1} $(2.303RT)^{-1}$; r = 0.99963							

[a] Vessel seasoned with allyl bromide and in the presence of cyclohexene or toluene inhibitor.

TABLE 6: Kinetic Parameters at 400.0 °C from the Experimental Results

substrate	10^4k_1 (s^{-1})	$\log A$ (s^{-1})	E_a (kJ/mol)	$\Delta S^{\ddagger}$ (J/(mol·K))	$\Delta H^{\ddagger}$ (kJ/mol)	$\Delta G^{\ddagger}$ (kJ/mol)
I	4.79 ± 0.55	13.73 ± 0.19	219.8 ± 2.5	2.85 ± 0.12	214.2 ± 2.5	212.3 ± 2.6
II	3.39 ± 0.77	13.37 ± 0.39	217.1 ± 5.1	−4.04 ± 0.24	211.5 ± 5.1	214.2 ± 5.3

corresponding Arrhenius equations are given in Table 5 (90% confidence coefficient from least-squares procedure).

Once the values for the activation energy (E_a) and the preexponential Arrhenius factor (A) are obtained, the activation enthalpies can be calculated from the equation

$$\Delta H^{\ddagger} = E_a - mRT \tag{6}$$

where m is the molecularity of the reaction, that is, the number of molecules of reactant per molecule of TS; in this case, m is equal to 1. On the other hand, the activation entropy is deduced from the relationship

$$A = (e^m\, kT/h)\exp(\Delta S^{\ddagger}/R) \tag{7}$$

With the use of eq 2, the $\Delta G^{\ddagger}$ value is obtained. Hence, the activation parameters $\Delta G^{\ddagger}$, $\Delta H^{\ddagger}$, and $\Delta S^{\ddagger}$ can be obtained from two independent sources: either from the experimental measurements with eqs 6, 7, and 2 or from the theoretical calculations as explained before. The kinetic data obtained from the experimental data of the hydroxyesters are included in Table 6.

4.2. Theoretical Results. The gas-phase decomposition of methyl glycolate was not theoretically studied because it was not possible to obtain a complete experimental kinetic study, as explained before.

The pyrolitic eliminations of **I** and **II** in the gas phase were studied from a theoretical point of view to obtain a complete picture and a deeper insight into the molecular mechanisms of the decompositions. The equilibrium geometries of **I** and **II** are depicted in Figure 1, including atom numbering. For **II**, two geometries are depicted, the first one related with **TS2** and **TS5** and the other related with **TS3** (see below). It is not clear which is the most stable conformation at the temperature used in the calculations (400 °C), although the differences are small. At MP2/6-31G** level, the first conformation is described as more stable (the Gibbs free energy difference between the two conformations is equal to 7.13 kJ·mol^{-1}); the second conformer has lower enthalpy than the first one by 12.23 kJ·mol^{-1}, but the entropic term is also lower by 28.76 J·mol^{-1}·K^{-1}. However, at MP2/6-31++G** level, the corresponding values for enthalpy, entropy, and Gibbs free energy differences are −6.67 kJ·mol^{-1}, 0.08 J·mol^{-1}·K^{-1}, and −6.72 kJ·mol^{-1}, respectively. Finally, at B3LYP/6-31+G** level, the values are −7.44 kJ·mol^{-1}, 2.82 J·mol^{-1}·K^{-1}, and −9.34 kJ·mol^{-1}, respectively, and hence the second conformation is described as more stable at the two last levels.

An exhaustive exploration of the PESs associated with the decomposition processes of **I** and **II** has been conducted, and the possible mechanisms have been characterized. In the case of **I**, we have found the TS related with the process experimentally described, **TS1** (Figure 2). The corresponding TV is mainly controlled by the simultaneous C2−C3, C3−O4, and O2−H2 breaking bonds, thus yielding directly the products in one step.

In the case of **II**, the equivalent TS has been characterized (**TS2**, Figure 2). In addition, other decomposition mechanisms have been found that can explain the paths yielding the byproducts experimentally observed. The acetone and methyl formate products can be reached in a two-step process: a first TS (**TS3**, Figure 3) yields acetone and a zwiterionic species, which in turn, through a second TS (**TS4**, Figure 3), renders methylformate. On the other hand, the methyl methacrylate can be obtained via the TS describing the direct water elimination from reactants (**TS5**, Figure 3).

4.2.1. Energetics and the Kinetic Parameters. The thermochemical data of products and byproducts relative to the reactants (ΔH, ΔS, and ΔG), obtained from the normal mode Gaussian 98 outputs as explained, are reported in Table 7. The activation parameters ($\Delta H^{\ddagger}$, $\Delta S^{\ddagger}$, and $\Delta G^{\ddagger}$), together with the calculated elementary first-order rate coefficients, corresponding to the decomposition reactions of **I** through **TS1** and of **II** through **TS2**, **TS3** and **TS4**, and **TS5**, are also included in Table 7.

The decompositions of the two compounds are endothermic processes; ΔH values are positive. But the entropy increments are large, and the global processes are favorable; ΔG values are always negative. The decomposition of **II**, to yield CO, CH_3OH, and CH_3COCH_3 is found to be themodynamically more favorable than the corresponding processes that yield either $HCOOCH_3$ and CH_3COCH_3 or H_2O and $CH_2CH(CH_3)$-$COOCH_3$.

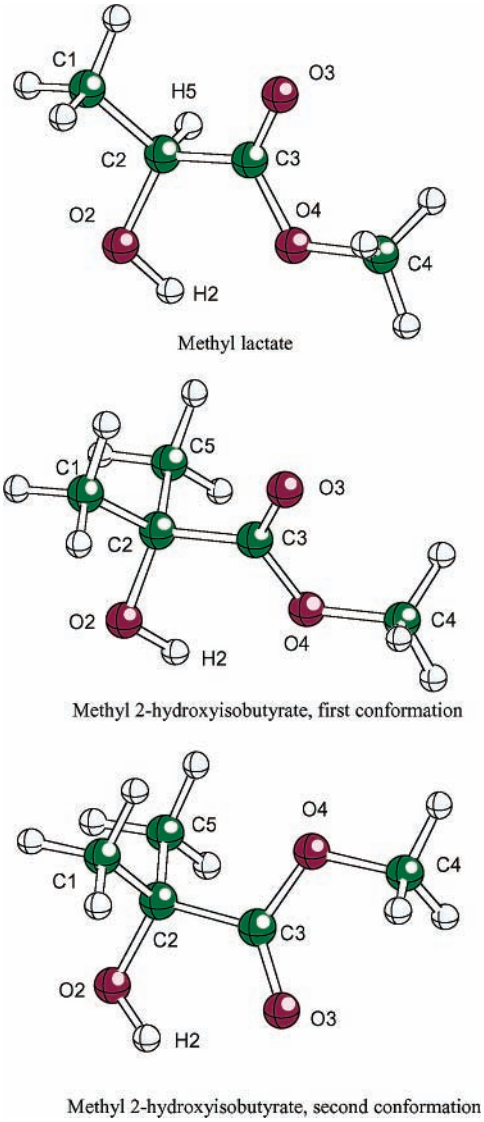

Figure 1. Structures of reactants, methyl lactate and methyl 2-hydroxyisobutyrate. For the last species, two conformations are shown.

When comparing the results obtained with the three different theoretical approaches used, we see significative differences in the values of the increments of enthalpy and entropy. In general, ΔH values are lower with the DFT approach than with MP2, and the same can be observed with respect to the ΔS values. However, the ΔG values in the main processes are found to be roughly independent of the theoretical level used. This is not observed in the case of the obtainment of the byproducts, for which differences rounding 30 kJ·mol^{-1} are obtained.

A comparison between the experimental and the theoretical values of $\Delta G^{\ddagger}$ for **TS1** and **TS2**, listed in Tables 6 and 7, respectively, shows that the best approach is the MP2/6-31++G** level, for which the differences between the experimental and theoretical values are ~3 kJ·mol^{-1}. The worst one is B3LYP/6-31+G**, for which the $\Delta G^{\ddagger}$ is clearly understimated for **TS2**. Therefore, the rate coefficient values obtained at the first level show quite a good agreement with experiment, while the values obtained with the last level are 1 order of magnitude larger than the experimental ones. For MP2/6-31G**, the results obtained agree quite well with experiment for **TS2** and slightly differ for **TS1**.

By using eq 6, one can obtain the Arrhenius activation energy, E_a, from the theoretical $\Delta H^{\ddagger}$ values and compare it with the experimental ones. For the three levels used, the E_a values

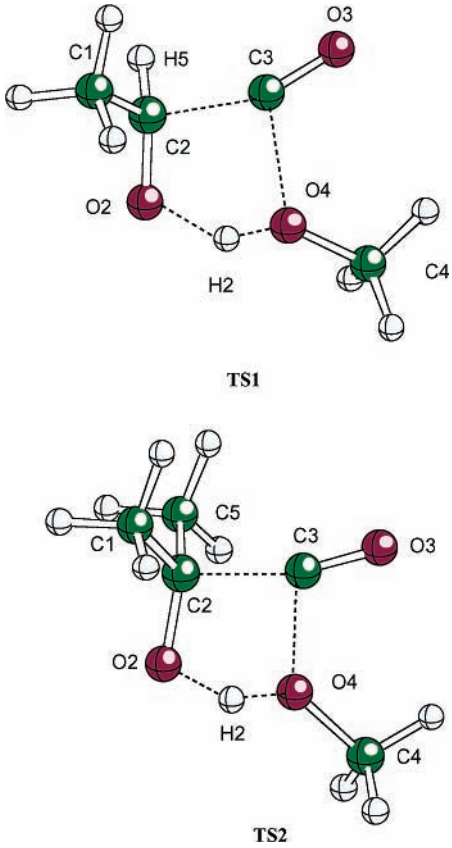

Figure 2. Structures of **TS1** and **TS2**.

obtained for **TS1** are 231.6 (MP2/6-31G**), 231.2 (MP2/6-31++G**), and 219.6 kJ·mol^{-1} (B3LYP/6-31+G**), while for **TS2** they are 228.1, 227.3, and 211.1 kJ·mol^{-1}. The B3LYP results agree better with the experiment than the MP2 values: the experimental values are 219.8 and 217.1 kJ·mol^{-1} for **TS1** and **TS2**, respectively.

One can then conclude in the present case that the DFT method describes very well the activation enthalpy and, consequently, the Arrhenius activation energy, E_a, and quite poorly the activation entropy. The MP2 methods, while describing poorly either the enthalpic or the entropic term, compensate these two errors, and a good value is obtained for the activation Gibbs free energy and rate coefficient. This seems to be a quite general trend, and we have tested that MP2 approaches render very good values for $\Delta G^{\ddagger}$ and k values in the gas-phase decompositions of different systems.[9−14]

In Figure 4, the experimental and theoretical Arrhenius plots for the main processes are presented. The values for log k were calculated by means of the corresponding frequency calculations of TSs and reactants at the same temperatures used for the experimental plot, as well as by using the theoretically obtained values for E_a and A, eqs 6 and 7, and the Arrhenius equation:

$$\log k = \log A - E_a/(2.303RT) \qquad (8)$$

The same results were obtained, as expected. For the **I** decomposition (Figure 4a), it can be seen that the four lines are roughly parallel, due to the good agreement in the Arrhenius activation energies between experimental and theoretical values, specially for the B3LYP/6-31+G** level. The lines do not coincide, thus reflecting the differences in the Arrhenius preexponential factor, A: the experimental value for log A is 13.73, and the MP2/6-31G**, MP2/6-31++G**, and B3LYP/6-31+G** values are, respectively, 14.04, 14.35, and 14.14. In

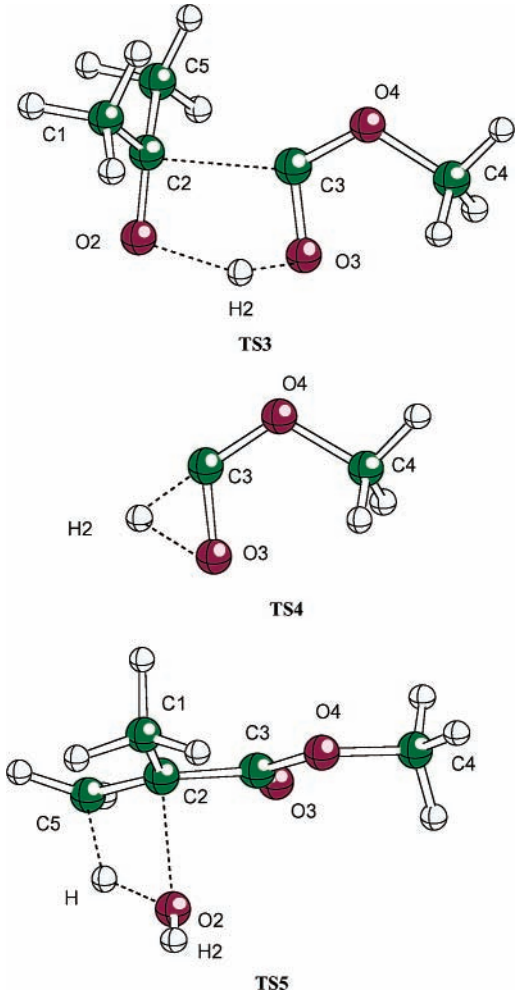

Figure 3. Structures of **TS3**, **TS4**, and **TS5**.

Figure 4b, the corresponding Arrhenius plots for the decomposition of **II** to give CO, methanol, and acetone are presented. As before, the lines are roughly parallel, while the corresponding values for log *A* are 13.37 (experimental), 14.00 (MP2/6-31G**), 14.34 (MP2/6-31++G**), and 14.22 (B3LYP/6-31+G**).

Several byproducts have been found in the decomposition process of **II**, and we have characterized possible mechanistic paths leading to such byproducts. In Figure 5a, a schematic representation of the Gibbs free energy values for all stationary points found, relative to reactants, for the decomposition process of **II** is presented at MP2/6-31++G** and at B3LYP/6-31+G** levels. The MP2/6-31G** level renders results similar to that at MP2/6-31++G** and the results are not shown.

Starting from the reactant in its first conformation, the pathway through **TS2** to yield the main products is the more favorable, as expected. The alternative paths to the byproducts are kinetically unfavored: the first alternative path would pass through **TS3**, the intermediate zwitterionic species, and **TS4** to give methyl formate plus acetone. The barrier to pass over **TS3** (the limiting step) is 28.7 kJ/mol greater than the barrier to pass over **TS2** at MP2/6-31++G** level. This alternative path would explain the minority observation of methyl formate as byproduct.

On the other hand, the passage through **TS5** to yield water and methyl methacrylate is even less favorable, the barrier being 67.8 kJ/mol greater than the **TS2** barrier at MP2/6-31++G** level.

For the sake of completeness, we have also studied analogous alternative mechanisms for the decomposition of **I**, at MP2/6-31G** level (Figure 5b). In this case, the obtainment of methyl

TABLE 7: Relative Enthalpies (ΔH, kJ/mol), Entropies (ΔS, J/(mol·K)), and Gibbs Free Energies (ΔG, kJ/mol) to the Corresponding Reactants in Their Most Stable Conformations, Activation Enthalpies ($\Delta H^{\ddagger}$, kJ/mol), Entropies ($\Delta S^{\ddagger}$, J/mol·K), and Gibbs Free Energies ($\Delta G^{\ddagger}$, kJ/mol) to the Corresponding Reactants or Intermediates, and First-Order Rate Coefficients (k, s^{-1})[a]

	ΔH	ΔS	ΔG
products from **I**, $CO + CH_3OH + CH_3CHO$	107.8	353.4	−130.1
	(99.3)	(353.9)	(−138.9)
	[97.4]	[337.9]	[−130.1]
products from **II**, $CO + CH_3OH + CH_3COCH_3$	102.2	369.2	−146.3
	(88.5)	(344.8)	(−143.6)
	[71.6]	[328.0]	[−149.2]
byproducts from **II**, $HCOOCH_3 + CH_3COCH_3$	59.2	227.4	−93.9
	(50.7)	(174.0)	(−66.5)
	[14.4]	[168.1]	[−98.8]
byproducts from **II**, $H_2O + CH_2CH(CH_3)COOCH_3$	73.2	175.3	−44.8
	(59.0)	(182.4)	(−63.8)
	[38.7]	[170.4]	[−76.0]

	$\Delta H^{\ddagger}$	$\Delta S^{\ddagger}$	$\Delta G^{\ddagger}$	k
TS1	226.1	8.9	220.1	1.18×10^{-4}
	(225.6)	(14.7)	(215.7)	(2.57×10^{-4})
	[214.0]	[10.7]	[206.8]	$[1.25 \times 10^{-3}]$
TS2	222.5	8.1	217.0	2.02×10^{-4}
	(221.7)	(14.6)	(211.9)	(5.03×10^{-4})
	[205.6]	[12.2]	[197.4]	$[6.79 \times 10^{-3}]$
TS3	243.2	23.1	227.6	3.05×10^{-5}
	(237.1)	(−5.2)	(240.6)	(2.99×10^{-6})
	[193.9]	[−11.6]	[201.7]	$[3.13 \times 10^{-3}]$
TS4	121.8	3.4	119.5	7.48×10^{3}
	(123.9)	(3.4)	(121.6)	(5.14×10^{3})
	[132.1]	[5.6]	[128.4]	$[1.53 \times 10^{3}]$
TS5	296.8	0.3	296.6	1.36×10^{-10}
	(284.0)	(6.3)	(279.8)	(2.75×10^{-9})
	[257.9]	[8.9]	[251.9]	$[3.97 \times 10^{-7}]$

[a] All values in this table have been theoretically calculated at MP2/6-31G**, at MP2/6-31++G** (in parentheses), and at B3LYP/6-31+G** (in brackets).

formate can be afforded through **TS6** (depicted in Figure 6) followed by **TS4**, the barrier over **TS6** being 30.9 kJ/mol greater than the barrier associated with **TS1**. At the same theoretical level, for **II**, the difference between the barriers through **TS3** and **TS2** is only 10.6 kJ/mol, and therefore, it is more probable to obtain the byproducts in the last case than in the first one, in which, in fact, the putative byproducts are not experimentally detected. The second alternative path, in the case of **I**, would lead to water and methyl propionate via **TS7** (Figure 6). The barrier is 76.2 kJ/mol greater than the corresponding **TS1** barrier, a similar value to that obtained at the same theoretical level for the decomposition of **II** via **TS5** (79.5 kJ/mol). Experimentally the formation methyl propionate is not detected, although experimental confirmation exists of the obtainment of methyl methacrylate. This trend could not be explained on theoretical grounds, based on the energetic values.

4.2.2. Geometries and Transition Vectors. TVs and geometries for the transition structures corresponding to the decomposition processes (**TS1** and **TS2**), as well as those related with the byproduct appearance (**TS3**, **TS4**, and **TS5**) and with the putative byproducts of methyl lactate (**TS6** and **TS7**), are reported in Table 8. Further information on TSs (the whole set of geometric parameters, the force constants, all positive

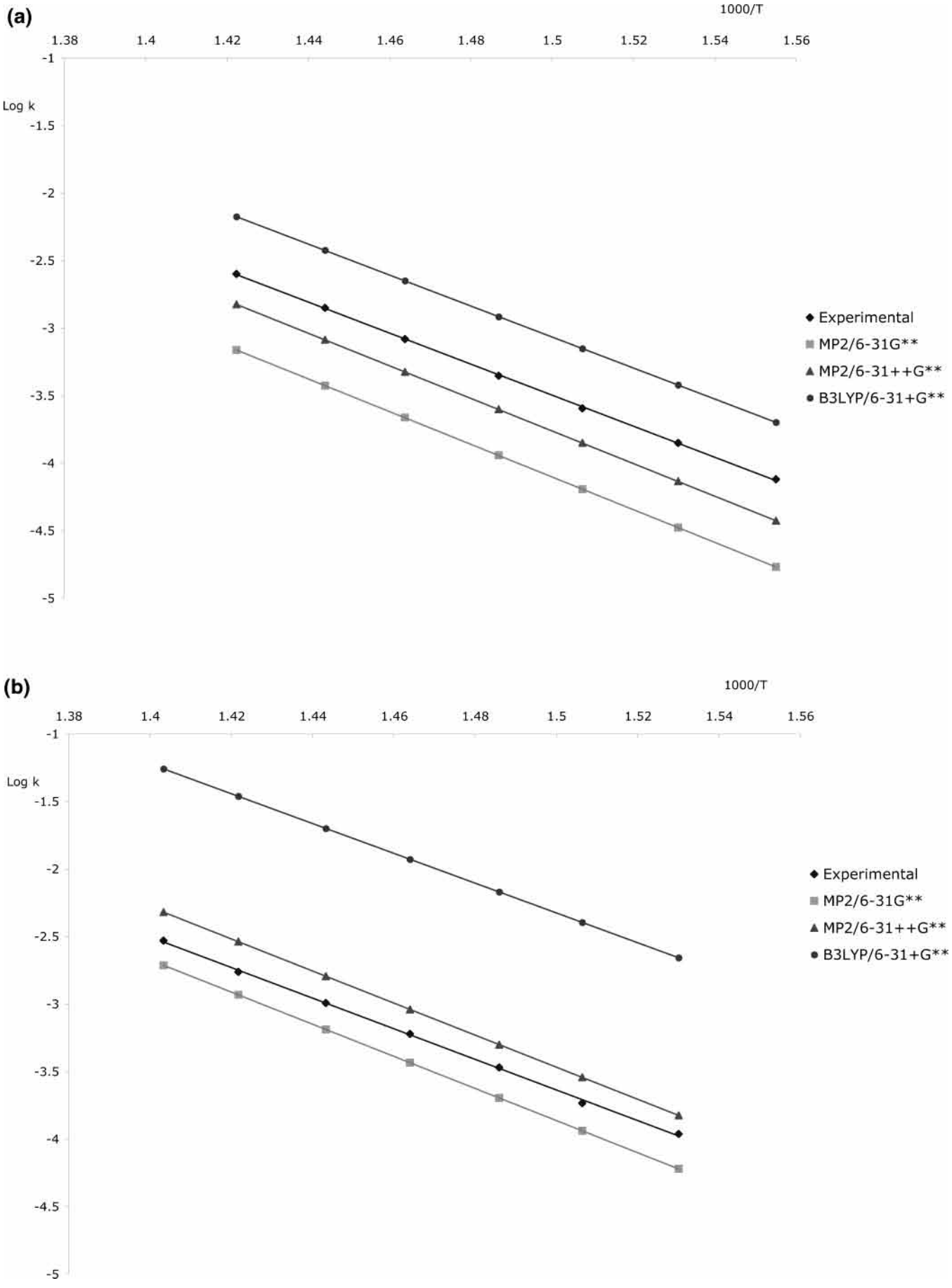

Figure 4. Arrhenius plots obtained from experimental and theoretical data, log k (s^{-1}) versus $1000/T$ (K^{-1}): (a) decomposition of **I** through **TS1**; (b) decomposition of **II** through **TS2**.

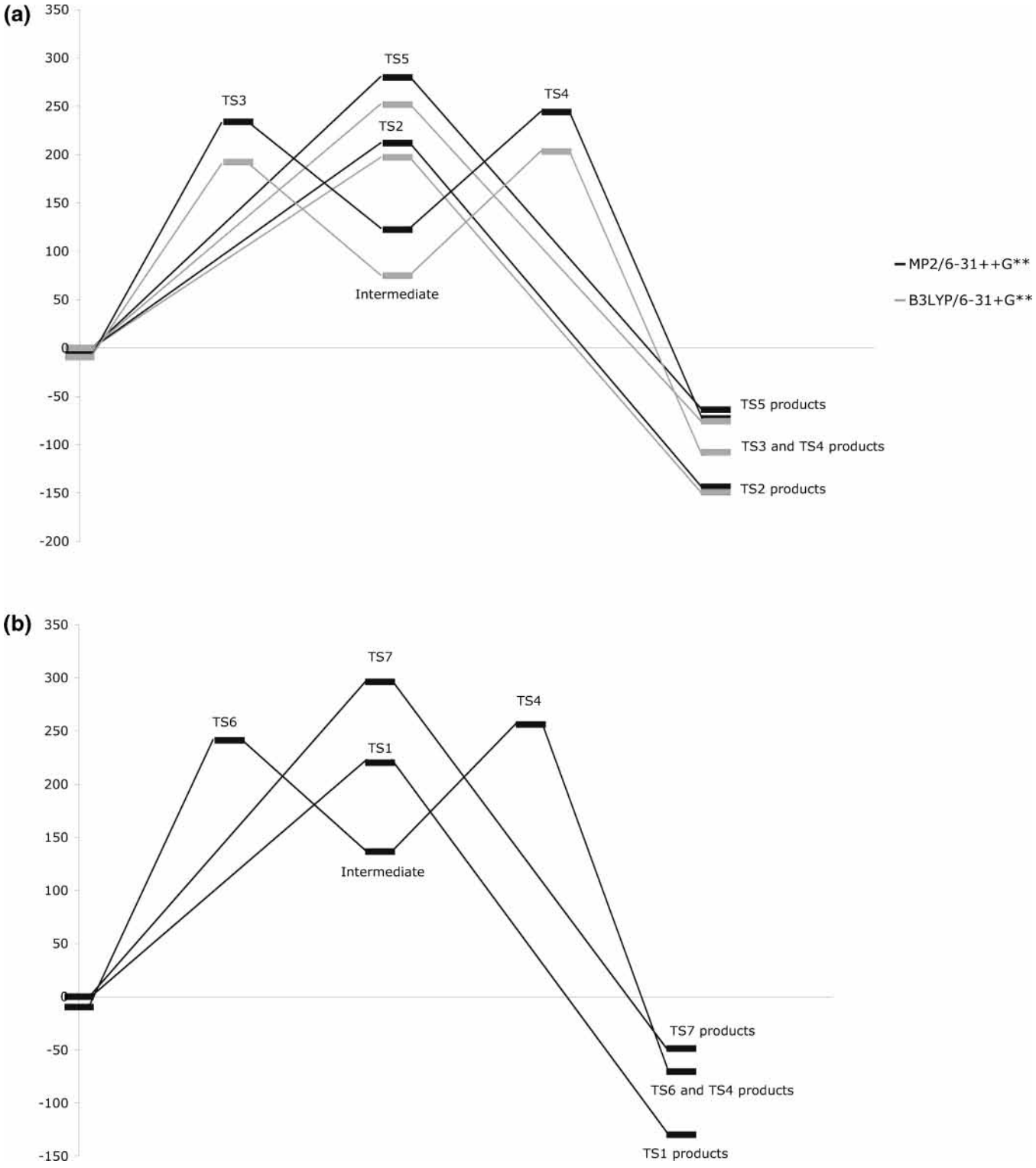

Figure 5. Gibbs free energy profiles at 673.15 K relative to reactants: (a) decomposition of **II** relative to reactants in its first conformation (see Figure 1); (b) decomposition of **I** relative to reactants in the conformation shown in Figure 1.

eigenvalues, or all vibrational frequencies) is available from the authors on request (andres@exp.uji.es; safont@exp.uji.es).

For **TS1** and **TS2** (see Table 8 and Figure 2), the main components of TV are the C2−C3, O2−H2, and C3−O4 distances. These components correspond to the decomposition processes. In addition, the O4−C3−C2 and O3−C3−C2 bond angles also have a significant participation in the TV, due to the separation of the three resulting molecules. The C2−O2 motion slightly participates in the TV; this bond evolves from single to double while the elimination process takes place.

The geometric parameters for **TS1** and **TS2** displayed in Table 8 correspond with a concerted molecular mechanism, and the TSs are late, closer to the products than to the reactant. Thus, the distances for the breaking bonds C2−C3, O2−H2, and C3−O4 are ca. 1.8, 1.5, and 1.97 Å, respectively, while the H2−O4 forming bond distance (data not shown in Table 8) is 1.03 Å. The distance for the bond that evolves from single to double, C2−O2, is ca. 1.3 Å. The simultaneity of the breaking and forming bonds can be better analyzed by using the bond order evolution and the synchronicity values (see below).

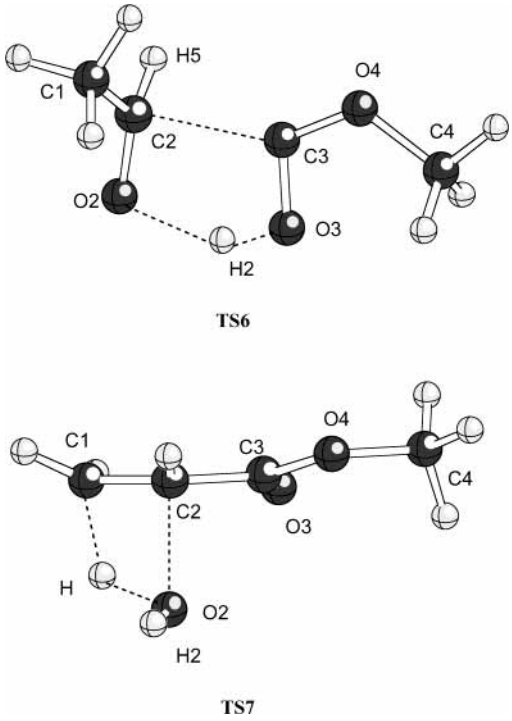

Figure 6. Structures of **TS6** and **TS7**.

For **TS3** and **TS6** (see Table 8 and Figures 3 and 6), the bond distances that participate significantly in the TV are the C2−C3 and O2−H2 breaking bonds, as well as the O4−C3−C2 bond angle. This reaction pathway corresponds to the formation of acetone or acetaldehyde and a zwitterionic species $HOCOCH_3$. An analysis of the geometric parameters values shows a concerted and late character for these TSs. The H2−O3 bond distance (data not shown in Table 8) is 1.02 Å.

The imaginary frequency values are between 500i and 620i cm^{-1} for **TS1** and **TS2**, depending on the computing level, and between 230i and 272i cm^{-1} for **TS3** and **TS6**, indicating that these stationary points are mainly associated with the heavy atom motions. It must be noted that the qualitative description of the decomposition processes is independent of the computing method used and also that the geometric values are not affected by the theoretical level. This fact points out that all theoretical approaches used are adequate for an accurate description of the processes in what refers to TVs and geometries.

TS4 is associated with the conversion of the intermediate to formaldehyde (see Figure 3 and Table 8). The TV is mainly controlled by the H2−O3 bond distance, as well as the H2−O3−C3 bond angle. The fluctuation pattern describes the H2 motion; the imaginary frequency value is high because the H motion dominates the process.

Finally, **TS5** and **TS7** (see Figures 3 and 6 and Table 8) are related with the dehydration of the starting reactant to give the corresponding alkene. The main TV components are the C−C distance that evolves from single to double (C2−C5 in **TS5**; C2−C1 in **TS7**) in antiphase with the O2−C2 bond breaking distance, as well as with the H−C5 (or H−C1 in **TS7**) distance, where H refers to the hydrogen atom leaving the methyl carbon at C5 (or C1). Also, the O2−C2−C5 and the H−C5−C2 bond angles have significant contributions to the TV for **TS5** and the same for the O2−C2−C1 and H−C1−C2 bond angles for **TS7**. The imaginary frequency values are very high, thus indicating that the fluctuation pattern is associated with the water elimination, particularly with the H motions.

4.2.3. Bond Order Analysis. To better analyze the extent of bond breaking or bond forming along the characterized reaction pathways, the bond order (B) concept has been used.[41−43] The Wiberg bond indices[44] have been computed by using the natural bond orbital (NBO)[45,46] analysis as implemented in Gaussian 98.[30] Several breaking/forming bond processes are involved in the mechanisms, and the nature of each step can be monitored by means of the synchronicity (Sy) concept proposed by Moyano et al.,[47] using the following expression:

$$\mathrm{Sy} = 1 - \frac{\sum_{i=1}^{n} \frac{|\delta B_i - \delta B_{\mathrm{av}}|}{\delta B_{\mathrm{av}}}}{2n - 2} \tag{9}$$

In eq 9, n is the number of bonds directly involved in the reaction, and the relative variation of the bond index is obtained from

$$\delta B_i = \frac{B_i^{\mathrm{TS}} - B_i^{\mathrm{R}}}{B_i^{\mathrm{P}} - B_i^{\mathrm{R}}} \tag{10}$$

where the superscripts TS, R, and P refer to the TS, reactant, and product of each step, respectively. The average value is therefore

$$\delta B_{\mathrm{av}} = n^{-1} \sum_{i=1}^{n} \delta B_i \tag{11}$$

Synchronicities calculated from expression 9 and the Wiberg bond indices[44] of the breaking/making bond processes, obtained at MP2/6-31++G** level, are reported in Table 9. The percentage of evolution of the bond order through each chemical step has been calculated by using

$$\%\mathrm{Ev} = \delta B_i \times 100 \tag{12}$$

The results are also included in Table 9.

For **TS1**, the percentages of evolution of the bond orders are within a range of 29%−80%, thus describing a somewhat asynchronous TS. The displacement of H2 atom is the more advanced motion (80.4% evolution), while the C2−C3 breaking bond and the C2−O2 bond, which evolves from single to double, are late, displaying a small evolution percentage. Then, the extension of the O2−H2 bond with initial migration of the hydrogen atom to O4 and the C3−O4 breaking bond with a high evolution percentage value (74.4%) can be seen as the driving forces for the decomposition process. The synchronicity value of 0.777 shows that the reaction pathway can be described as concerted and slightly asynchronous.

A very similar analysis can be made in what refers to **TS2**, thus showing that the decompositions of either **I** or **II** take place via the same mechanisms, through equivalent TSs. The similar values obtained for the rate coefficients for the two systems can be explained on the basis of the present bond order analysis.

On the other hand, **TS3** has a larger synchronous character than **TS2**; the corresponding Sy value is 0.93. The C2−O2 evolution from single to double bond and the C2−C3 breaking bond processes are the latest for this TS with 58.3% and 66.4% evolution, respectively. The more advanced bond order evolution corresponds to the O2−H2 breaking, 86.1% evolution. All percentages of evolution are within a narrow range of 58.3%−86.1%, reflecting the highly synchronous character or this TS. The next TS of this path, **TS4**, also shows a highly synchronous

TABLE 8: Imaginary Frequency (freq, cm^{-1}), Main Components of the TV (C, au), and Corresponding Geometric Parameters (G, bonds in Å, Angles and Dihedrals in deg) for the Indicated TSs, MP2/6-31G Values[a]**

	TS1		TS2	
freq	566.30i (532.04i) [508.78i]		599.42i (555.53i) [619.66 i]	
	C	G	C	G
C2−C3	0.556 (0.645) [0.646]	1.758 (1.771) [1.821]	0.653 (0.657) [0.666]	1.768 (1.780) [1.866]
C2−O2	−0.153 (−0.154) [−0.151]	1.296 (1.298) [1.291]	−0.154 (−0.160) [−0.146]	1.303 (1.305) [1.299]
O2−H2	0.504 (0.419) [0.406]	1.456 (1.499) [1.445]	0.405 (0.423) [0.388]	1.429 (1.469) [1.377]
C3−O4	0.455 (0.469) [0.462]	1.963 (1.969) [1.918]	0.451 (0.453) [0.441]	1.954 (1.960) [1.878]
H2−O2−C2	0.106 (0.099) [0.113]	96.52 (98.13) [100.79]	0.095 (0.094) [0.091]	96.99 (98.24) [101.32]
O4−C3−C2	−0.193 (−0.137) [−0.145]	91.19 (91.92) [92.90]	−0.141 (−0.139) [−0.150]	91.42 (91.92) [92.41]
O3−C3−C2	0.294 (0.102) [0.162]	149.34 (151.64) [151.52]	0.079 (0.098) [0.214]	147.87 (150.72) [152.20]
O2−C2−C1−H5	−0.195 (−0.221) [−0.213]	−141.39 (−141.28) [−141.97]	−0.251 (−0.225) [−0.229]	−139.22 (−139.31) [−141.27]
O3−C3−C2−O2	−0.066 (−0.185) [−0.233]	107.84 (122.02) [140.19]	−0.220 (−0.156) [−0.122]	104.20 (116.71) [139.40]

	TS3		TS6	
freq	264.87i (272.36i) [235.43i]		230.58i	
	C	G	C	G
C2−C3	0.821 (0.818) [0.801]	2.202 (2.192) [2.218]	0.791	2.224
O2−H2	0.230 (0.370) [0.423]	1.553 (1.576) [1.506]	0.438	1.603
H2−O2−C2	0.115 (0.092) [0.083]	99.88 (100.13) [101.50]	0.073	99.33
O4−C3−C2	0.301 (0.236) [0.219]	147.89 (146.76) [146.76]	0.222	148.72
O3−C3−C2	−0.162 (−0.125) [−0.117]	98.20 (99.06) [97.81]	−0.111	97.81
O2−C2−C1−C5[b]	−0.288 (−0.266) [−0.265]	−154.44 (−153.78) [−153.51]	−0.263	−159.06
C3−C2−O2−C5[b]	0.126 (0.115) [0.120]	−103.19 (−103.52) [−103.64]	0.124	−95.76

	TS4	
freq	1897.21i (1893.95i) [1934.28i]	
	C	G
O3−C3	−0.242 (−0.236) [−0.255]	1.315 (1.316) [1.303]
H2−O3	0.708 (0.716) [0.696]	1.209 (1.215) [1.222]
O3−C3−O4	0.245 (0.231) [0.232]	118.32 (118.90) [119.66]
H2−O3−C3	−0.613 (−0.612) [−0.626]	58.64 (58.94) [59.17]

	TS5		TS7	
freq	2201.73i (2061.01i) [1466.86i]		2219.61i	
	C	G	C	G
C2−C5[c]	−0.259 (−0.317) [−0.252]	1.416 (1.412) [1.416]	−0.320	1.413
O2−C2	0.441 (0.359) [0.360]	1.891 (1.959) [2.102]	0.353	1.846
H−C5[c]	0.639 (0.568) [0.662]	1.395 (1.348) [1.276]	0.552	1.423
O2−C2−C5[c]	−0.300 (−0.455) [−0.277]	92.38 (89.56) [83.77]	−0.489	94.12
H2−O2−C2	0.192 (0.094) [0.393]	113.15 (127.60) [151.69]	0.087	110.45
H−C5−C2[c]	−0.312 (−0.444) [−0.302]	74.94 (78.50) [86.33]	−0.439	73.90
O2−C2−C5−C1[d]	−0.120 (−0.107) [−0.124]	107.54 (106.56) [101.07]	−0.088	104.37
H2−O2−C2−C3	0.246 (0.077) [0.017]	129.53 (115.36) [62.13]	0.076	130.72

[a] MP2/6-31++G** and B3LYP/6-31+G** values are given in parentheses and brackets, respectively. [b] H5 instead of C5 in **TS6**. [c] C1 instead of C5 in **TS7**. [d] C1 instead of C5 and H5 instead of C1 in **TS7**.

character with a Sy value of 0.923, and the percentages of evolution of the main bonds breaking or forming stand in a range of 47%−64%; the TS has an intermediate character between its reactant and product.

TS5, corresponding to the obtainment of water and methyl methacrylate, also shows a very synchronous character and an intermediate nature between reactant and products, Sy value of 0.835; the percentages of evolution of the main bond orders in a range of 34%−61.4%.

Finally, an analysis of the NBO charges for **I** shows a large negative charge at C1 (−0.62) and at O2, O3, and O4 (−0.81, −0.70 and −0.67, respectively). C4 bears also a negative charge (−0.21). Positive charges mainly appear at C3 (0.96) and H2 (0.51) centers. At **TS1**, the negative charge at C1 has been slightly increased to −0.66; the charge on O2 and O4 has also been increased to −0.90 and −0.85, respectively, while the negative charge on O3 has somewhat been decreased to −0.57. The charge on C4 is maintained. The positive charges on C3 and H2 have been slightly modified to 0.89 and 0.58, respectively. The largest variation between reactant and TS atomic charges corresponds to the positive charge on C2, which evolves from 0.04 at reactant to 0.28 at TS. The smooth charge redistribution between reactant and TS indicates that the breaking and forming bond processes are coupled, hence supporting the conclusion that the process can be described as concerted. The slight asynchrony is mainly reflected in the positive charge increment on H2, in the negative charge increment on O2, and in the C2 charge variation.

A very similar analysis can be done for **II**, first conformation, and the corresponding **TS2**: At reactant, large negative charges are found at C1 and C5 (−0.61 and −0.62, respectively), as well as at the oxygen atoms O2, O3, and O4 (−0.81, −0.70 and −0.68, respectively), and also at C4 (−0.21). At C2, a positive charge can be sensed (0.20). The main positive charges are located on C3 (0.97) and H2 (0.51). At **TS2**, the charges have been slightly modified: a small increment in the negative charges on C1 (−0.65), C5 (−0.65), O2 (−0.91), and O4 (−0.85) is found. The charge on C4 has been maintained

TABLE 9: Wiberg Bond Indices (B_i) and Percentage of Evolution through the Chemical Process (%Ev) of the Bond Indices at the Indicated TSs Calculated by Means of Eq 12 and the Synchronicity Value (Sy) Obtained from Eq 9[a]

TS1

	C2−C3	C3−O4	O4−H2	O2−H2	C2−O2
B_i^R	0.96	0.99	0.01	0.72	0.92
B_i^{TS}	0.68	0.25	0.51	0.14	1.23
%Ev	28.9	74.4	68.5	80.4	34.6
Sy			0.777		

TS2

	C2−C3	C3−O4	O4−H2	O2−H2	C2−O2
B_i^R	0.95	0.99	0.01	0.72	0.91
B_i^{TS}	0.67	0.26	0.50	0.15	1.21
%Ev	29.8	73.3	66.3	78.6	34.8
Sy			0.785		

TS3

	C2−C3	C3−O3	O3−H2	O2−H2	C2−O2
B_i^R	0.95	1.68	0.01	0.70	0.92
B_i^{TS}	0.32	1.20	0.55	0.10	1.42
%Ev	66.4	75.1	77.0	86.1	58.3
Sy			0.930		

TS4

	H2−O3	O3−C3	H2−C3
B_i^R	0.70	1.04	0.00
B_i^{TS}	0.28	1.42	0.43
%Ev	63.9	55.3	46.9
Sy		0.923	

TS5

	C2−C5	C5−H	H−O2	C2−O2
B_i^R	0.99	0.93	0.00	0.92
B_i^{TS}	1.31	0.44	0.26	0.36
%Ev	35.0	53.1	34.0	61.4
Sy		0.835		

[a] The results obtained at MP2/6-31++G** level are reported.

(−0.21), and the charge on O3 has been reduced (−0.57). The positive charges on C3 (0.90) and H2 (0.58) are quite close to the reactant values, as before, and the more significative charge variation takes also place at C2, the charge of which increases to 0.44. Therefore, the process is correctly described as concerted and slightly asynchronous.

5. Conclusions

This work can be considered a collaborative project between experimental and theoretical research groups. The methyl 2-hydroxypropionate and methyl 2-hydroxyisobutyrate have been pyrolyzed, and the corresponding rate coefficients have been determined by pressure measurements and quantitative chromatographic analysis. The kinetic parameters and the reactive potential energy surfaces at MP2/6-31G**, MP2/6-31++G**, and B3LYP/6-31+G** calculation levels have been theoretically obtained. The first-order rate coefficients were then evaluated in terms of transition-state theory, and the theoretical results have been compared with the experimental data. From the combination of experimental and theoretical studies, the following conclusions can be drawn: (1) The experimental data show that the decompositions are homogeneous and unimolecular, and follow first-order rate laws, which have been determined. (2) The decomposition processes, via five-membered cyclic transition structures, **TS1** and **TS2**, yield the corresponding products in one step. The molecular mechanisms can be described as concerted and slightly asynchronous. (3) An analysis of bond orders and NBO charges suggests that the extension of the O2−H2 bond with initial migration of the hydrogen atom to O4 seems to be the driving force for the decomposition processes, either at **TS1** or at **TS2**. (4) Alternative mechanisms have been found that can explain the byproduct formation in the case of the methyl 2-hydroxyisobutyrate decomposition. A two-step mechanism via **TS3** and **TS4** would explain the acetone and methyl formate formation. This path is calculated to be unfavored with respect to the main path, explaining the very small formation of the corresponding byproducts. On the other hand, a one-step mechanism via the four-center **TS5** has been found that can explain the water and methyl methacrylate formation. This mechanism is even less favored, which explains the even smaller byproduct formation. (5) An equivalent theoretical study has been made on the possibility of analogous byproduct formation for the methyl 2-hydroxypropionate decomposition. This study, based on energetic grounds, renders that the obtainment of methyl formate plus acetone from methyl 2-hydroxyisobutyrate is more probable than the obtainment of methyl formate and acetaldehyde from methyl 2-hydroxypropionate. However, it is not explained why methyl 2-hydroxyisobutyrate dehydrates to yield methyl methacrylate, while water and methyl propionate are not experimentally detected in the decomposition of methyl 2-hydroxypropionate. (6) For the main processes, the analysis and comparison of the calculated and experimental kinetic parameters and Arrhenius plots point out the validity of the theoretical approaches. A good agreement is achieved between the theoretical and experimental results.

Acknowledgment. We are grateful for financial support to DGI (Project BQU2000-1425-C03-02), as well as to Fundació Caixa Castelló-Bancaixa (Project P1 1A2002-04). Computer facilities of the Servei d'Informàtica of the Universitat Jaume I are also acknowledged.

References and Notes

(1) Chuchani, G.; Rotinov, A. *Int. J. Chem. Kinet.* **1989**, *21*, 367.
(2) Chuchani, G.; Domínguez, R. M.; Rotinov, A. *Int. J. Chem. Kinet.* **1991**, *23*, 779.
(3) Chuchani, G.; Martín, I.; Rotinov, A.; Domínguez, R. M. *J. Phys. Org. Chem.* **1993**, *6*, 54.
(4) Chuchani, G.; Martín, I.; Rotinov, A.; Domínguez, R. M.; Pérez, I. M. *J. Phys. Org. Chem.* **1995**, *8*, 133.
(5) Chuchani, G.; Domínguez, R. M. *Int. J. Chem. Kinet.* **1995**, *27*, 85.
(6) Chuchani, G.; Rotinov, A.; Domínguez, R. M. *J. Phys. Org. Chem.* **1996**, *9*, 787.
(7) Chuchani, G.; Martin, I. *J. Phys. Org. Chem.* **1997**, *10*, 121.
(8) Chuchani, G.; Domínguez, R. M.; Rotinov, A.; Martin, I. *J. Phys. Org. Chem.* **1999**, *12*, 612.
(9) Safont, V. S.; Moliner, V.; Andrés, J.; Domingo, L. R. *J. Phys. Chem. A* **1997**, *101*, 1859.
(10) Domingo, L. R.; Andrés, J.; Moliner, V.; Safont, V. S. *J. Am. Chem. Soc.* **1997**, *119*, 6415.
(11) Domingo, L. R.; Picher, M. T.; Andrés, J.; Safont, V. S.; Chuchani, G. *Chem. Phys. Lett.* **1997**, *274*, 422.
(12) Domingo, L. R.; Picher, M. T.; Safont, V. S.; Andrés, J.; Chuchani, G. *J. Phys. Chem. A* **1999**, *103*, 3935.
(13) Rotinov, A.; Chuchani, G.; Andrés, J.; Domingo, L. R.; Safont, V. S. *Chem. Phys.* **1999**, *246*, 1.
(14) Chuchani, G.; Rotinov, A.; Andrés, J.; Domingo, L. R.; Safont, V. S. *J. Phys. Chem. A* **2001**, *105*, 1869.
(15) Chuchani, G.; Rotinov, A.; Domínguez, R. M.; Martín, I. *J. Phys. Org. Chem.* **1996**, *9*, 348.

(16) Capon, B.; McManus, S. P. *Neighboring Group Participation*; Plenum Press: New York, 1976; Vol. 1.
(17) Chuchani, G. In *Pyrolysis of Organic Halides*; Patai, S., Rappoport, Z., Eds.; Wiley: Chichester, 1995; Supplement D2.
(18) Domínguez, R. M.; Rotinov, A.; Chuchani, G. *J. Phys. Chem.* **1986**, *90*, 6277.
(19) Swinbourne, E. S. *Aust. J. Chem.* **1958**, *11*, 334.
(20) Maccoll, A. *J. Chem. Soc.* **1965**, 965.
(21) Glasstone, K. J.; Laidler, K. J.; Eyring, H. *The Theory of Rate Processes*; McGraw-Hill: New York, 1941.
(22) Laidler, K. J. *Theories of Chemical Reaction Rates*; McGraw-Hill: New York, 1969.
(23) Heidrich, D.; Kliesch, W.; Quapp, W. *Properties of Chemically Interesting Potential Energy Surfaces*; Springer-Verlag: New York, 1991.
(24) Marcus, R. A. *J. Chem. Phys.* **1965**, *43*, 1598.
(25) Forst, W. *Theory of Unimolecular Reactions*; Academic Press: New York, 1973.
(26) Truhlar, D. G.; Garrett, B. C. *Acc. Chem. Res.* **1980**, *13*, 440.
(27) Truhlar, D. G.; Isaacson, A. D.; Garrett, B. *Theory of Chemical Reaction Dynamics*; Chemical Rubber Co.: Boca Raton, FL, 1985.
(28) Tapia, O.; Andres, J. *J. Mol. Struct. (THEOCHEM)* **1995**, *335*, 267.
(29) Tapia, O.; Andrés, J.; Stamato, F. L. M. G. In *Solvent Effects and Chemical Reactivity*; Tapia, O., Bertrán, J., Eds.; Kluwer Academic Publishers: Dordrecht, The Netherlands, 1996; Vol. 17.
(30) Frisch, M. J.; Trucks, G. W.; Schlegel, H. B.; Scuseria, G. E.; Robb, M. A.; Cheeseman, J. R.; Zakrzewski, V. G.; Montgomery, J. A., Jr.; Stratmann, R. E.; Burant, J. C.; Dapprich, S.; Millam, J. M.; Daniels, A. D.; Kudin, K. N.; Strain, M. C.; Farkas, O.; Tomasi, J.; Barone, V.; Cossi, M.; Cammi, R.; Mennucci, B.; Pomelli, C.; Adamo, C.; Clifford, S.; Ochterski, J.; Petersson, G. A.; Ayala, P. Y.; Cui, Q.; Morokuma, K.; Malick, D. K.; Rabuck, A. D.; Raghavachari, K.; Foresman, J. B.; Cioslowski, J.; Ortiz, J. V.; Stefanov, B. B.; Liu, G.; Liashenko, A.; Piskorz, P.; Komaromi, I.; Gomperts, R.; Martin, R. L.; Fox, D. J.; Keith, T.; Al-Laham, M. A.; Peng, C. Y.; Nanayakkara, A.; Gonzalez, C.; Challacombe, M.; Gill, P. M. W.; Johnson, B. G.; Chen, W.; Wong, M. W.; Andres, J. L.; Head-Gordon, M.; Replogle, E. S.; Pople, J. A. *Gaussian 98*; Gaussian, Inc.: Pittsburgh, PA, 1998.
(31) Schlegel, H. B. *J. Comput. Chem.* **1982**, *3*, 214.
(32) Schlegel, H. B. *J. Chem. Phys.* **1982**, *77*, 3676.
(33) McIver, J. W., Jr. *Acc. Chem. Res.* **1974**, *7*, 72.
(34) Fukui, K. *J. Phys. Chem.* **1970**, *74*, 4161.
(35) González, C.; Schlegel, H. B. *J. Phys. Chem.* **1990**, *94*, 5523.
(36) González, C.; Schlegel, H. B. *J. Chem. Phys.* **1991**, *95*, 5853.
(37) Hehre, W. J.; Radom, L.; Schleyer, P. v. R.; Pople, J. A. *Ab Initio Molecular Orbital Theory*; John Wiley & Sons: New York, 1986.
(38) McQuarrie, D. *Statistical Mechanics*; Harper & Row: New York, 1986.
(39) Benson, S. W. *The foundations of chemical kinetics*; McGraw-Hill: New York, 1960.
(40) Methyl formate was only formed in very small amount (2%) as an elimination from **II**. Our working pyrolytic temperatures were 380−440 °C. The literature reports the pyrolysis of methyl formate as follows: (i) Formation of methanol and carbon monoxide[48] ($HCOOCH_3 \rightarrow CH_3OH + CO$). In this case, the reaction was carried out from 368 to 550 °C and was found to be heterogeneous and retarded by the product of the reaction. (ii) Formation of formaldehyde ($HCOOCH_3 \rightarrow 2CH_2O$) in the early stages of decomposition or formation of formaldehyde, hydrogen, and carbon monoxide ($HCOOCH_3 \rightarrow CH_2O + H_2 + CO$) if the reaction was carried out over long periods of time.[49] The reaction was carried out from 476 to 500 °C, the decomposition is molecular, and no free radical is involved.
(41) Varandas, A. J. C.; Formosinho, S. J. F. *J. Chem. Soc., Faraday Trans. 2* **1986**, 282.
(42) Lendvay, G. *J. Mol. Struct. (THEOCHEM)* **1988**, *167*, 331.
(43) Lendvay, G. *J. Phys. Chem.* **1989**, *93*, 4422.
(44) Wiberg, K. B. *Tetrahedron* **1968**, *24*, 1083.
(45) Reed, A. E.; Curtiss, L. A.; Weinhold, F. *Chem. Rev.* **1988**, *88*, 899.
(46) Reed, A. E.; Weinstock, R. B.; Weinhold, F. J. *J. Chem. Phys.* **1985**, *83*, 735.
(47) Moyano, A.; Pericàs, M. A.; Valentí, A. *J. Org. Chem.* **1989**, *54*, 573.
(48) Steacie, E. W. *Proc. R. Soc. London, Ser. A* **1930**, *127*, 314.
(49) Jain, D. V. S.; Murwaha, B. S. *Indian J. Chem.* **1969**, *7*, 901.